01 Jan 2023

Practical Imaging Applications Of Wettability Contact Angles On Kuwaiti Tight Carbonate Reservoir With Different Rock Types

Saleh Al-Sayegh

Ralph E. Flori
Missouri University of Science and Technology, reflori@mst.edu

Waleed Al-Bazzaz

Sohaib Kholosy

et. al. For a complete list of authors, see https://scholarsmine.mst.edu/geosci_geo_peteng_facwork/2114

Recommended Citation

S. Al-Sayegh et al., "Practical Imaging Applications Of Wettability Contact Angles On Kuwaiti Tight Carbonate Reservoir With Different Rock Types," *Society of Petroleum Engineers - Gas and Oil Technology Showcase and Conference, GOTS 2023*, Society of Petroleum Engineers, Jan 2023.
The definitive version is available at https://doi.org/10.2118/214165-MS

SPE-214165-MS

Practical Imaging Applications of Wettability Contact Angles on Kuwaiti Tight Carbonate Reservoir with Different Rock Types

Saleh Al-Sayegh, Missouri University of Science and Technology / Kuwait Oil Company; Ralph Flori, Missouri University of Science and Technology; Waleed Al-Bazzaz and Sohaib Kholosy, Kuwait Institute for Scientific Research; Hasan Al-Saedi, Missouri University of Science and Technology; Abdulaziz Abbas and Ali Qubian, Kuwait Oil Company

 DOI 10.2118/214165-MS

This paper was prepared for presentation at the Gas & Oil Technology Showcase and Conference held in Dubai, UAE, 13 - 15 March, 2023.

Abstract

This study focuses on a tight carbonate reservoir which is located in Northern Kuwait and is classified as an unconventional reservoir. A practical imaging technique of wettability contact angle (θ°) presents "big data" as well as relative-permeability (K_{rw} and K_{ro}) measurements. Also, modeling, through rock image technology, the vast well-documented grain/pore boundary morphology available inside fresh rock fragments have achieved good results. Conventional laboratory relative-permeability experiments are expensive and time-consuming. This study introduces a novel method to measure/calculate relative permeability through fast, less expensive, non-destructive, and environmentally friendly techniques of imaging technology. One tight carbonate reservoir is selected, imaged, processed, analyzed, and then modeled using several pore diameter morphological models. The images are captured using a backscattered electron microscopy BSE-SEM technology analyses.

In this study, two-dimensional images are used to characterize the morphology of selected samples grains and pores, using a two-step technique. In the first step, the image is captured using a backscattered electron detector (BSE), digital electron microscopy imaging, and pore-counting processing technology. All of the sample grain/pore features captured in the image are reported in micrometer units. In the second step, the pore area of such features is scanned using image analysis software that can accurately measure several morphological parameters of pore and grain spaces.

A robust technique of visual estimate is used, which has the advantage of speeding the image analysis process. The visual analysis software tool counts different pores and counts grains and also measures their shapes and sizes which are crucial for relative permeability calculations. Several pore morphological models have been considered for optimum accuracy comparisons, including pore/grain relationships (area/perimeter), pore contact angle (θ), and pore count. Relative permeability is calculated based on the area of the pore/grain features measured from two-dimensional images.

The study objectives are to accurately measure the wettability contact angle of huge pore geometries using 2D image technology to understand the nature of the pore network in the candidate reservoir. To study the relative permeability of internal influences of pore and grain morphology needed for enhanced oil recovery/improved oil recovery (EOR/ IOR) future programs. And, finally, to measure relative permeability faster and more accurately.

Introduction

Classic Kuwaiti carbonate reservoir is known to exist as a thick and fractured limestone formation in North Kuwait that shows good production (1). However, in this formation, production is getting difficult. In the North field, referred to in this study as "LIMESTONE" formation averages about 430 feet of net-oil-pay. It exhibits high porosity – about 18% – and a low matrix permeability between 0.0001 - 10's millidarcies.

Porosity and permeability petrophysical reservoir general knowledge justified the agenda of maximizing the production from LIMESTONE by characterizing the relative permeability as well as the wettability for future IOR production programs. A total of 27 vertical sequences core samples were proposed for relative permeability curves construction study. First, this study proposes the investigation of wettability contact angle at the pore/ grain level. Then, it continues to create its subsequent relative permeability(s) measurements based on the cumbersome captured pore/ grain morphology contact angles. Wettability contact angles are presented as big data and they are manifested at the pore-scale. These thousands reported contact angles are then modeled using 2D digital imaging technologies and morphological pre-logics. 27-core chips from carbonate native samples covering the entire carbonate formation thickness of the LIMESTONE reservoir are the candidate representations for EOR/ IOR unconventional reservoir characterization using this novel technique.

The main objective of this project is to conduct a laboratory trial to use the novel method of using pore scale measurement and modeling using 2D digital imaging to estimate wettability contact angle (θ °) and subsequent relative permeability curves (K_{rw} and K_{ro}) in the static physics of the reservoir rock in the native state. The obtained results will be analyzed for further assessment of the applicability and validation of the method. The study objectives are: first, to accurately measure Wettability contact angle of huge pore geometries using 2D image technology. Further, to study relative permeability action of internal influences of pore and grain morphology. In due action, measure relative permeability faster and more accurate approach.

This study proposes a detailed characterization of this formation to expedite future reservoir planning and development. Since the world's demand for oil is increasing, and the price of oil is also increasing, reservoir engineers are looking forward to developing this reservoir as soon as possible. This study is to offer information trial of reservoir characterization application that suggests a novel proposed method for relative-permeability and wettability contact angle determination for tight carbonate oil reservoirs.

This relative permeability measurements introduce the preliminary laboratory results as a trial inception for a novel application of the method in LIMESTONE formation in North Kuwait.

Background

Wettability is a complex phenomenon for it is difficult to yield accurate measurements, control quantitative repeatability, shorten the time of experimental data generation, and high cost of analysis (2–10). A new and novel technique using digital imaging technologies has addressed all these issues. Captured rock physics is deterministically reported and big-morphological-quantified data is measured. This technique can be applied to any worldwide EOR/ IOR reservoir candidate (11–14).

Relative permeability is the ratio of the effective permeability of a particular fluid at a particular saturation to the absolute permeability of that fluid at total saturation (15–21). Relative permeability is dependent upon

pore geometry, wettability, fluid distribution, and fluid saturation history (22–24). It is requested to study the wettability of a reservoir for projects where secondary and/or tertiary recovery is being considered.

Recent studies show that the majority of the permeability in the northern Kuwait field is contributed to the large, unconventional cavern pores, which means that the knowledge of the matrix pore network is wholly unknown (24–29). As a result, more information is needed at the pore level to evaluate the matrix. This knowledge will assist in understanding the nature of the reservoir and how better to drain it.

In this study, 2-dimensional images are used to characterize the morphology of the grains and pores, using a two-step process (8, 14). In the first step, the image is captured. In the second step, the area and average pore contact area of such features are scanned using image analysis software that can accurately measure several morphological parameters of pore and grain spaces as indicated in Figure 1. This study utilizes area measurement and contact angle as the criterion parameter for all analyses. Morphological features are calculated based on area and contact angle, which brings the level of information accuracy into two dimensions. This information, which is considered "Big Data," is taken and analyzed to find answers that enable cost and time reductions.

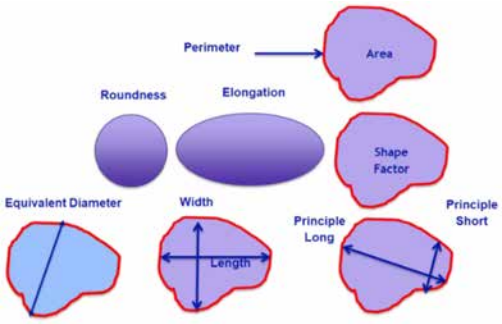

Figure 1—Pore/ grain boundary morphological reservoir wettability contact angle and relative permeability model.

Novel Digital Imaging Technique Advantage

- Conventional laboratory relative permeability, as well as wettability experiments, are expensive and time-consuming.
- This study introduces a novel (static) method to measure wettability and relative permeability through fast, less expensive, and environmentally friendly techniques of imaging technology.
- Static Method requires no fluids to be introduced into the rock samples, but measures natural attributes and features available in the rock through pores and grain morphology of which porosity and permeability are accurately measured and big data is reported in detail.
- Core samples are selected, 2D imaged, processed, analyzed, and then modeled using several pore diameter morphological models.
- The images are captured using SEM at different magnification scales.
- In this incepted research study, wettability characterization (quantitatively) is considered a deterministic microscopic approach based on measuring the contact angle of actual pore size and distribution.
- An innovative morphological approach to capture 2D images is critical for mapping pore geometry contact angle.
- Discover new wettability relationships and/or configurations.
- It encourages the identification and investigation of boundary conditions (limits, extremes, and cutoffs).

Equipment used for the analytical solution is imaging by static experimental data in SEM

1. Backscattered Scattered Electron Microscopy (SEM).
2. Image processing software.
3. Relative Permeability Global Database Suite.
4. Relative Permeability Correlations Suite.
5. Hearn PseudoRelative Permeability Analysis software.

Project Description and Methodology

The practicality in measurement will include:

1. Capturing grain/ pore geometry at 2D level for 7 rock types.
2. Image Processing using point counting method and generating big data.
3. Grain/ pore wettability contact angle measurement.
4. Porosity maps.
5. Grain diameter maps.
6. Absolute permeability calculations.
7. Connate water saturation (S_{wc}) and residual oil saturation (S_{or}) estimation
8. Developing 2D-digital relative permeability curves.

The equations used for this study are available in Table 1 for estimating the relative permeabilities LIMESTONE reservoir in the presence of two phases of oil and water is described by the following:

Table 1—Formulation of models.

Parameter	Method	Units	Approach	Description	Comments
Pore Area	Σ Pore Area	μ-m^2	Visual Counting	Measured	Accurate
Grain Area	Σ Grain Area	μ-m^2	Visual Counting	Measured	Accurate
Wettability Contact Angle θ°	Rough edges between pore and grain	(θ°) Degrees	Visual Counting	Measured	Accurate
Porosity	$\phi = \frac{\sum PoreArea}{\sum PoreArea + \sum GrainArea}$	Fraction	Summation/ Statistical	Calculated	Low Error
Initial Water Saturation	$Swc = \frac{\tau(1)}{\tau(Total)}$	Fraction	By Class Area Strong Water Wet Definition	Calculated/ Statistical/ Averaging	Avoid Circular or Triangular Shape Simplicity
Residual Oil Saturation)	$Sor = \frac{\tau(10)}{\tau(Total)}$	Fraction	By Class Area Strong Oil Wet Definition	Calculated/ Statistical/ Averaging	Avoid Circular or Triangular Shape Simplicity
Water Relative Permeability	$k_{ro}^{ow} = 1.2624 \left(\frac{So-Sorw}{1-Sorw}\right) \left[\frac{So-S_{orw}}{1-Swi-Sorw}\right]^2$	Fraction	Modified Brook/Corey Ibrahim/ Koederitz Honapour/ Koederitz/ Harvey	Calculated/ Statistical/ Averaging	Confidant
Oil Relative Permeability	$k_{ro}^{og} = 0.93752 \left(\frac{So}{1-Swi}\right)^4 \left[\frac{So-S_{org}}{1-Swi-Sorg}\right]^2$	Fraction	Modified Brook/Corey Ibrahim/ Koederitz Honapour/ Koederitz/ Harvey	Calculated/ Statistical/ Averaging	Confidant
Grain Diameter	$GrainDiameter = \frac{I}{1.32}$	μ-m	Kumar& Cui Sieve Method	Calculated	Originally Applied for mm-scale Grain Particles
Absolute Permeability	$k = 5.6281 \cdot \frac{d^2 \cdot \phi^3}{(1-\phi)^2}$	Milli-Darcy	Carmen & Kozeny	Calculated	Diameter & Porosity are Accurately Measured
Class Pore Area	Total Pore Areas Fitted in a Range of Pore Areas where MHR is Located	μ-m^2	Visual Counting	Measured	Accurate
Wettability	Θ = Pore Shapes and Morphology	Degrees	Pore/grain Orientations (New Proposal)	Measured	2-D 0° - 360°

The novel method promises advantages: low cost of implementation, estimation of S_{wc} and S_{or} values averaged in a large volume of big data from native core samples at the pore level.

Methodology

The study is spanned over 27 core samples, containing 7 rock types. The study is for one thick tight carbonate reservoir with one formation strata and several (7) rock types or 7 sub-reservoirs with limited types of strata's tight carbonates with well-defined rock types. First, we selected 27 core samples either end plugs or rock core fragments. Preferred in depths that are known for routine core analysis (RCA), where air permeability, and porosity, is statistically measured. The technique prefers that two core samples maybe three are selected for each rock type spanned in the rock type zone of interest.

The reservoir rock sample is imaged for unconventional wettability and relative permeability measurement. Each rock type is represented with, also, two to three samples throughout the rock type's thickness. The image is captured using a BSE-SEM digital electron microscopy imaging to characterize the morphology of the grains and pores boundaries. The morphology area of grain/ pore features is captured and then scanned using image analysis software to measure several morphological parameters twice for each selected image – once for grain morphology and once for pore morphology as shown in Figure 2. The "Big Data" is tabled for each sample for porosity, absolute permeability, contact angle, and relative permeability. Figure 3 depicts the logical experimental design for this study.

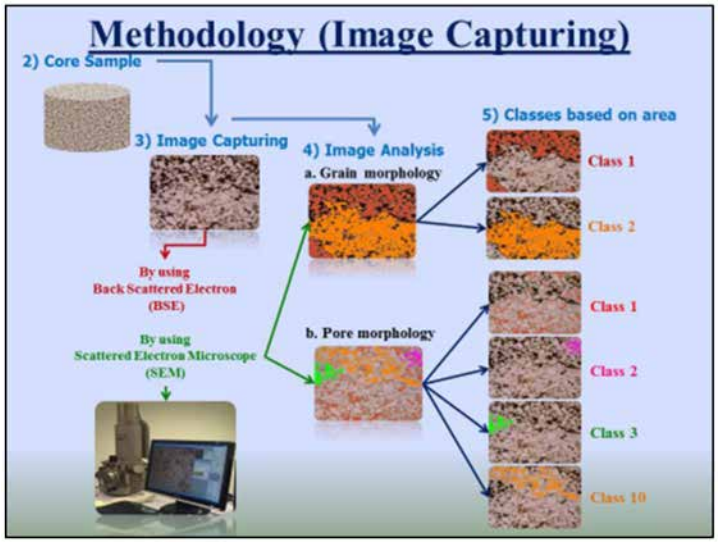

Figure 2—Image capturing procedure.

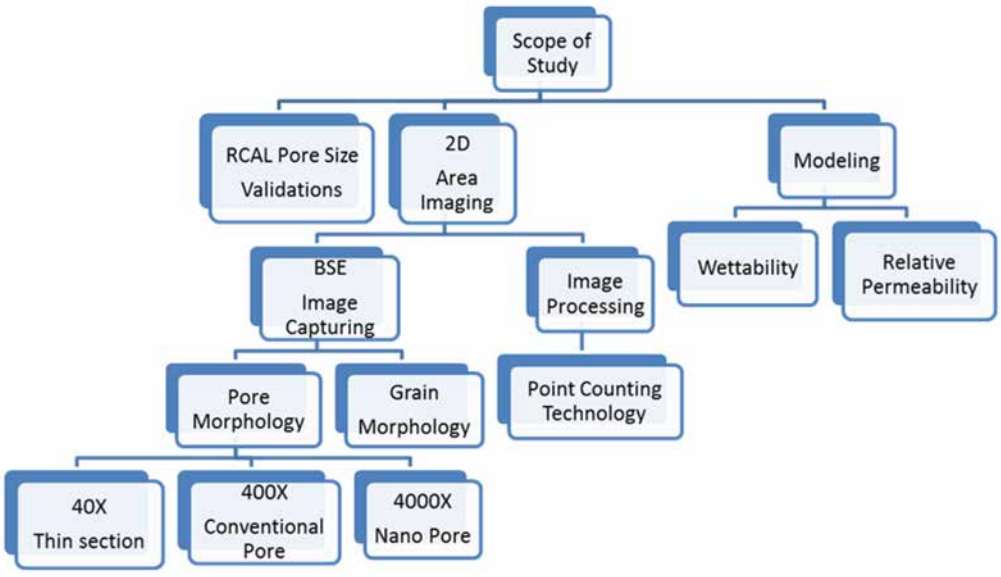

Figure 3—Logical experimental design.

Results

Analysis of routine and special core data relative permeability

Table 1 shows the empirical equations for estimating two-phase relative permeability in the LIMESTONE reservoir. Table 2 demonstrates a summary of the 7 rock types in LIMESTONE. All relative permeability

runs were on the global database and on Mohammed Ibrahim/ Koederitz model as well as Honapour/ Koederitz/ Harvey model as shown in Table 3 and Figures 4-5, respectively.

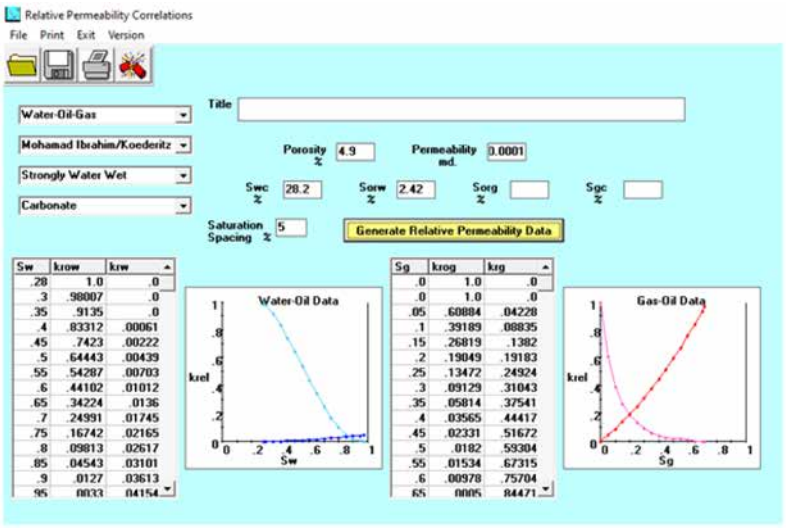

Figure 4—LIMESTONE data matching on global database using Mohammed Ibrahim/ Koederitz model.

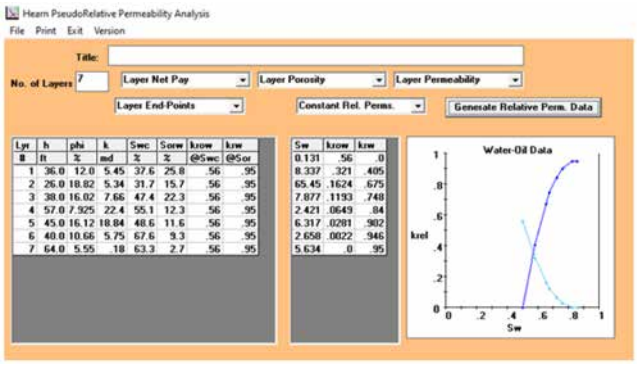

Figure 5—Overall LIMESTONE and 7 rock types summary on global database using hearn PseudoRelative Permeability multi rock types model.

Table 2—Summary of the 7 rock types in LIMSTONE

Rock Type No.	LIMSTONE	Top Depth (ft)	Bottom Depth (ft)	Rock Type Thickness (ft)	# of Plugs
1	A	7676	7712	36	36
2	B	7712	7738	26	21
3	C	7738	7776	38	36
4	D	7776	7833	57	55
5	E	7833	7878	45	40
6	F	7878	7918	40	41
7	G	7918	7982	64	13
			Σ	**306**	**242**

Table 3—LIMSTONE 7 rock types relative permeability of several pore geometry models.

Rock Type RT Name	Sample No.	Rock Type	Depth (ft)	Ibrahim/ Koederitz		Honapour/ Koederitz/ Harvey		Average			
								Ibrahim/ Koederitz		Honapour/ Koederitz/ Harvey	
				Krow	Krw	Krow	Krw	Krow	Krw	Krow	Krw
A	1	RT1	7684.2	0.933	10.200	0.897	0.000	0.847	2.615	0.651	0.438
A	2	RT1	7688.4	0.941	0.057	0.806	0.019				
A	3	RT1	7700.4	0.627	0.03889	0.162	1.725				
A	4	RT1	7708.6	0.886	0.163	0.741	0.009				
B	5	RT2	7713.25	0.873	0.116	0.857	0.000	0.761	11.286	0.574	0.124
B	6	RT2	7718.45	0.873	0.116	0.857	0.023				
B	7	RT2	7720.2	0.713	0.915	0.333	0.000				
B	26**	RT2	7721.9	0.762	0.018	0.527	0.001				
B	8	RT2	7735.3	0.582	55.265	0.297	0.595				
C	9	RT3	7741.45	0.823	22.489	0.323	0.000	0.855	4.618	0.478	0.014
C	10	RT3	7755.2	0.993	0.026	0.593	0.031				
C	11	RT3	7759.85	0.827	0.129	0.805	0.006				
C	27**	RT3	7767.1	0.730	0.069	0.303	0.005				
C	12	RT3	7773.8	0.903	0.379	0.362	0.026				
D	13	RT4	7777.7	0.854	0.142	0.526	0.124	0.816	14.678	0.472	0.038
D	14	RT4	7806	0.662	0.000	0.416	0.005				
D	15	RT4	7820.75	0.884	0.000	0.510	0.023				
D	16	RT4	7828.9	0.866	58.569	0.436	0.000				
E	17	RT5	7838.95	0.933	0.000	0.736	0.034	0.858	10.876	0.582	0.019
E	18	RT5	7848	0.912	0.105	0.649	0.036				
E	19	RT5	7854.4	0.722	0.127	0.392	0.004				
E	20	RT5	7878.2	0.865	43.272	0.552	0.000				
F	21	RT6	7887.8	0.867	0.000	0.297	0.007	0.817	0.059	0.545	2.863
F	22	RT6	7889.7	0.620	0.129	0.464	0.112				
F	23	RT6	7918.3	0.965	0.049	0.873	8.470				
G	24	RT7	7926.5	0.756	97.473	0.405	1.524	0.876	48.759	0.442	0.815
G	25	RT7	7933.8	0.996	0.044	0.478	0.107				

SEM-BSE Image capturing of 27 rock fragments after selection

According to Table 4 and Figures 6–18, LIMESTONE captured wettability contact angle images at mm 40X, μm 400X, and nm 4000X. The images were carefully selected and captured at three zoom magnifications, 40X which transfer the level of analysis in the millimeter scale. The 400X captures features in the micrometer scale and, finally, the 4000X studies pore, grain wall, and their interface important petrophysics phenomenon such as the wettability contact angle(s).

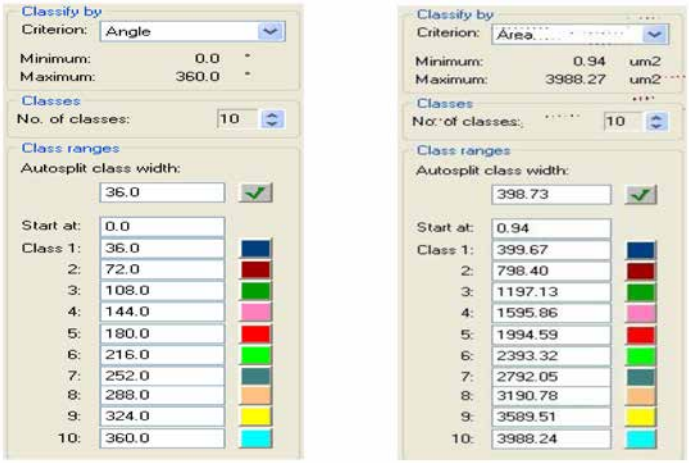

Figure 6—wettability contact angle classification key color identification. (a) classification by automatic refracted 10 degree angle range, (b) classification with its designated coloring of automatic pore area 10 class area mean and sum for estimation Swc and Sor

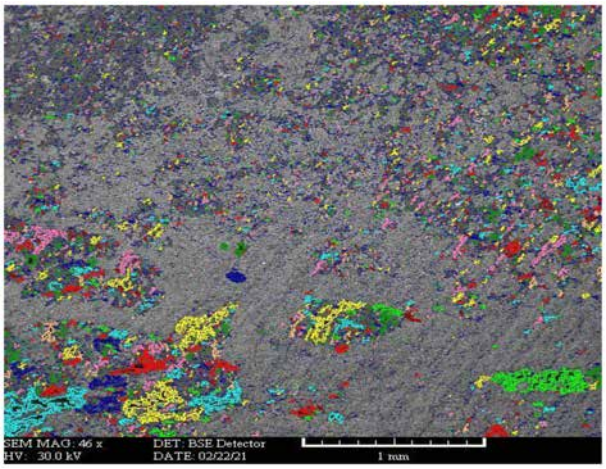

Figure 7—LIMESTONE has 10-wettability regions available in the 46X magnification. LIMESTONE total contact Angle (θ = 0° - 360°)-wettability regions with and total average contact angle θ = 40.876°.

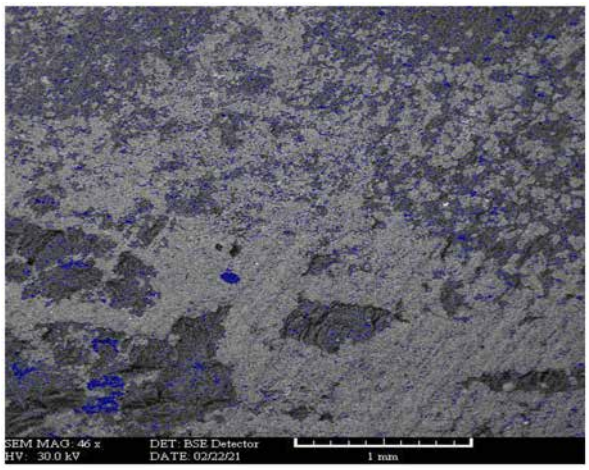

Figure 8—LIMESTONE class 1 (θ = 0° - 36°)-wettability regions with class average contact angle θ = 0.276°.

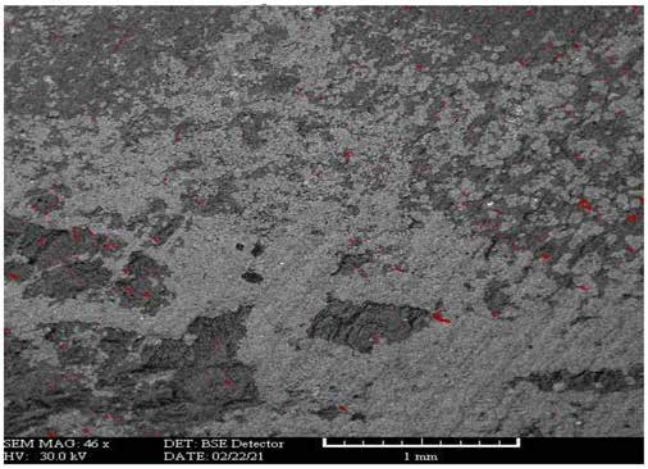

Figure 9—LIMESTONE class 2 (θ = 36° - 72°)-wettability regions with class average contact angle θ = 49.687°.

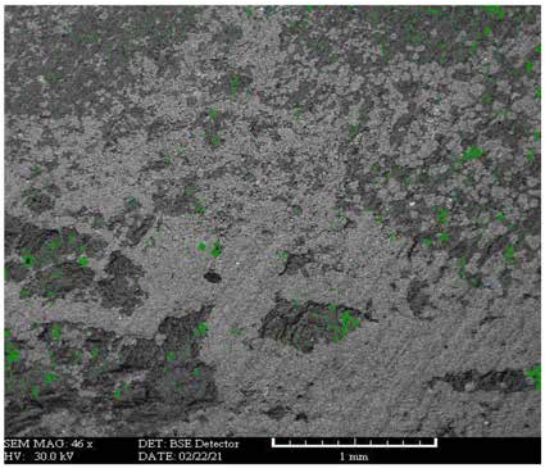

Figure 10—LIMESTONE class 3 (θ = 72° - 108°)- wettability regions with class average contact angle θ = 90.191°.

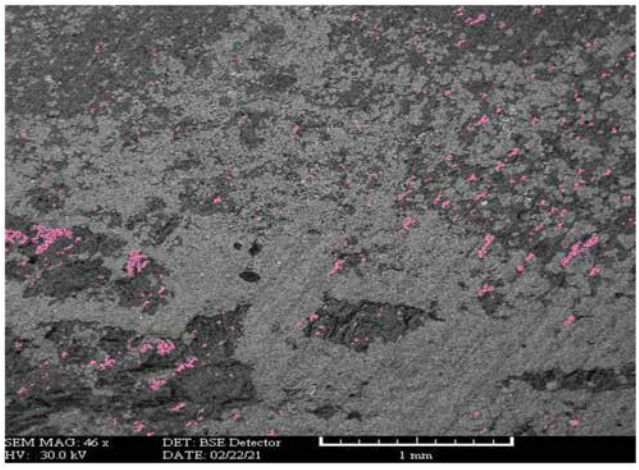

Figure 11—LIMESTONE class 4 (θ = 108° - 144°)- wettability regions with class average contact angle θ = 129.122°.

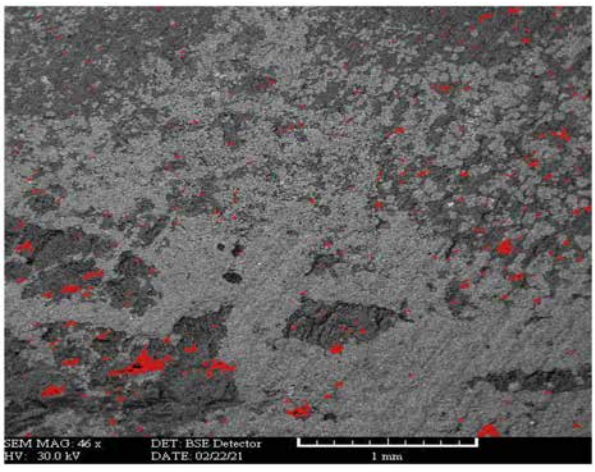

Figure 12—LIMESTONE class 5 (θ = 144° - 180°)- wettability regions with class average contact angle θ = 160.889°.

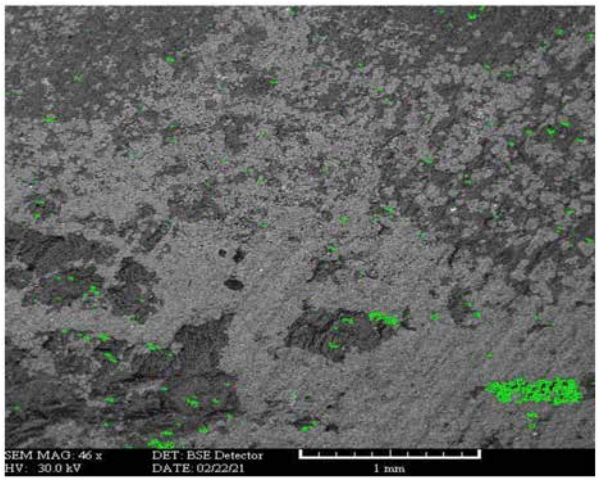

Figure 13—LIMESTONE class 6 (θ = 180° - 216°)- wettability regions with class average contact angle θ = 199.372° or 160.628°.

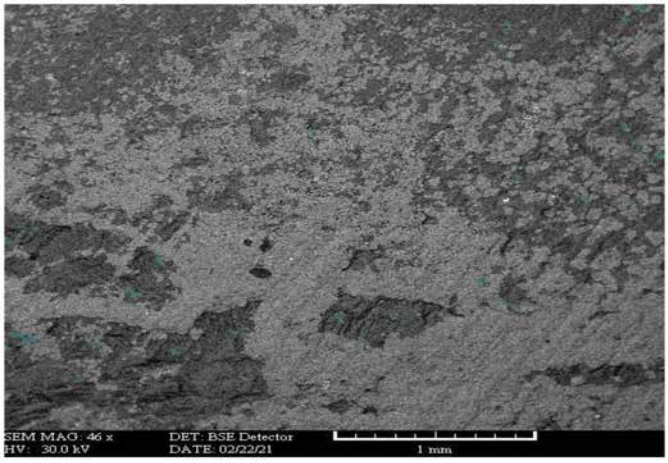

Figure 14—LIMESTONE class 7 (θ = 216° - 252°)- wettability regions with class average contact angle θ = 231.488° or 128.512°.

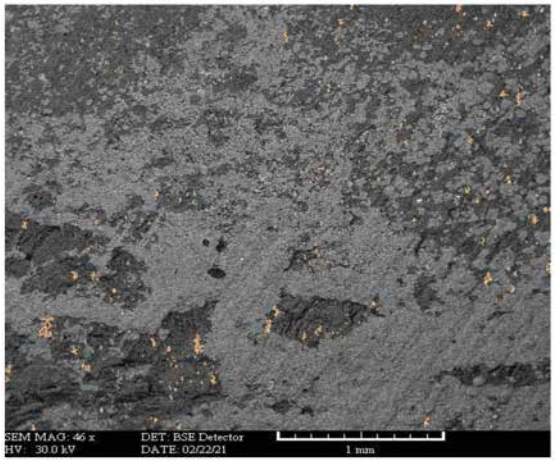

Figure 15—LIMESTONE class 8 (θ = 252° - 288°)- wettability regions with class average contact angle θ = 270.299° or 89.701°.

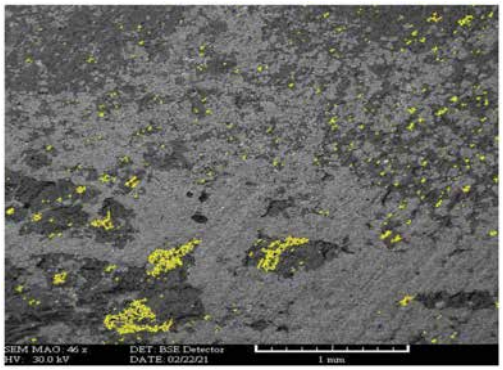

Figure 16—LIMESTONE class 9 (θ = 288° - 324°)- wettability regions with class average contact angle θ = 308.057° or 51.943°.

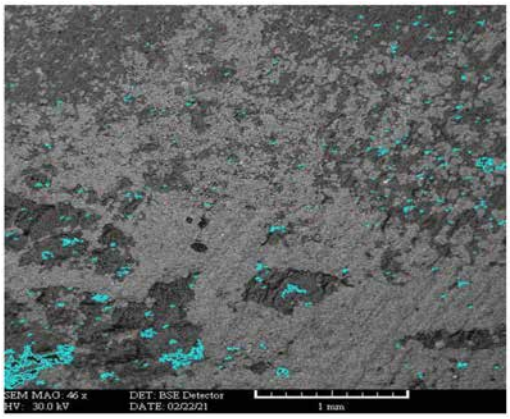

Figure 17—LIMESTONE class 10 (θ = 324° - 360°)- wettability regions with class average contact angle θ = 340.281° or 19.719°.

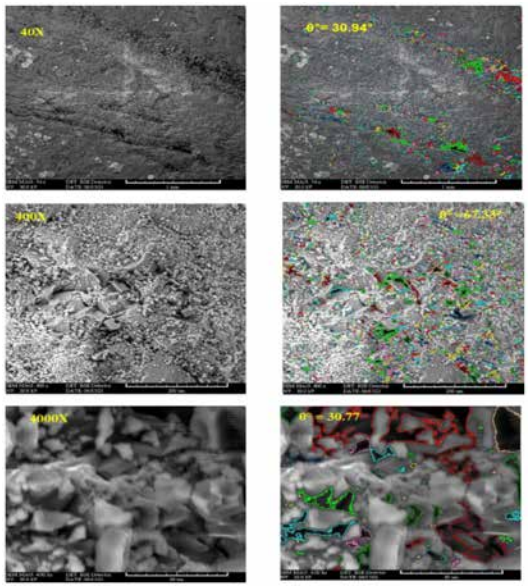

Figure 18—Practical capture of 2D-wettability contact angle for sample #10 (RT 3) and (depth 7755.2 ft) at X40 (θ = 30.94°), X400 (θ = 67.33°), X4000 (θ = 30.77°).

Table 4—Captured and measured contact angles for 27 LIMESTONE samples, contact angle θ° at 400X magnification (μm) is the pore throat size and is expected to be the corridor where oil is moving. Therefore, it is expected to be lesser water wet (so greater in value) than contact angles θ° at 4000X magnification (nm) and contact angle θ° at 40X magnification (mm).

						40X			400X			4000X		
			Sample No.	Rock Type	Depth	Average Contact Angle	Angle Area	Number of Angles	Average Contact Angle	Angle Area	Number of Angles	Average Contact Angle	Angle Area	Number of Angles
Rock Type RT Name	RT#	Reasons for Selection	#	Sequence	(ft)	θ°	μm^2	counts	θ°	μm^2	counts	θ°	μm^2	counts
A	1	Dolomite, tight matrix	1	RT1	7684.2	32.495	75.496	17245	59.787	2.971	5901	58.044	0.117	963
A	1	maximum perm	2	RT1	7688.4	26.607	83.455	7129	66.448	11.037	12047	76.591	1.571	1757
A	1	minimum perm	3	RT1	7700.4	26.686	122.256	10437	51.424	3.458	9580	26.929	0.094	2661
A	1	maximum por	4	RT1	7708.6	47.236	104.722	11930	69.143	16.334	5734	34.615	0.199	4627
B	2	Tight Matrix	5	RT2	7713.45	31.198	97.742	3991	50.235	3.896	14942	28.793	0.099	4002
B	2	maximum perm	6	RT2	7718.45	33.442	93.744	20732	56.859	81.033	1755	32.25	0.377	1702
B	2	maximum por	7	RT2	7720.2	89.829	293.1	3781	71.573	25.59	3583	62.687	2.457	272
B	2	KOC Selection	26**	RT2	7721.9	20.503	62.06	1941	52.773	3.067	7042	28.961	0.064	3246
B	2	minimum perm	8	RT2	7735.3	37.462	43.019	16174	70.348	5.538	3468	27.433	0.354	1503
C	3	minimum perm	9	RT3	7741.45	54.635	192.453	11811	91.41	13.994	2047	45.279	1.366	428
C	3	maximum perm	10	RT3	7755.2	30.949	59.767	12334	67.334	5.836	4965	30.768	0.441	1398
C	3	maximum por	11	RT3	7759.85	35.674	51.628	23045	35.983	2.135	2848	38.745	0.23	1337
C	3	KOC Selection	27**	RT3	7767.1	44.086	64.029	22439	60.58	5.16	5792	37.616	0.115	2177
C	3	Dolomite	12	RT3	7773.8	35.443	69.513	17864	71.436	9.194	6766	80.645	0.794	277
D	4	maximum GD	13	RT4	7777.7	39.183	111.642	24635	38.563	3.635	13015	65.79	0.565	597
D	4	maximum por	14	RT4	7806	50.291	184.792	4115	101.951	138.009	761	54.578	2.757	477
D	4	maximum perm	15	RT4	7820.75	47.447	117.893	22596	66.692	5.098	9310	32.985	0.064	6779
D	4	minimum perm	16	RT4	7828.9	35.906	81.987	25210	48.643	2.567	14442	34.52	0.042	10412
E	5	maximum perm	17	RT5	7838.95	37.053	88.408	18370	59.719	4.139	7830	30.102	0.151	3112
E	5	Dolomite	18	RT5	7848	41.254	69.712	11452	65.093	4.14	7687	33.224	0.218	3064
E	5	maximum por	19	RT5	7854.4	33.629	43.045	21855	51.358	3.012	10224	62.371	0.454	740
E	5	minimum perm	20	RT5	7878.2	38.541	48.718	21811	66.24	5.514	8581	34.935	0.178	1334
F	6	maximum por	21	RT6	7887.8	35.186	62.672	12042	66.934	4.36	9540	32.195	0.113	1701
F	6	maximum perm	22	RT6	7889.7	35.672	76.163	18072	55.508	3.402	8637	33.956	0.193	2285
F	6	inimum perm, Tight matr	23	RT6	7918.3	11.105	41.3	3215	44.642	2.22	6548	31.803	0.056	4571
G	7	inimum perm, Tight matr	24	RT7	7926.5	40.387	85.358	20665	38.851	1.834	4290	30.873	0.046	3285
G	7	ximum perm, maximum	25	RT7	7933.8	18.304	47.148	7701	52.198	3.09	6830	34.914	0.149	1331

This method is categorized by reflected angles between 0° - 360°. Figure 6 shows 10 classes of contact angles identified with distinct colors. Angles in blue (0° - 36°) are strong water wet (SWW) regions and angles in red (144° - 180°) are identified as being strong oil-wet (SOW).

Analysis of 7 images at a micrometer scale (400X) for 2D porosity (Φ) and permeability (k) measurements

According to Table (5 and 6) and Figure 19-, LIMESTONE Captured Average Grain Diameter (Blue-Maps) images at the scale of 400X magnification. The grain diameter is automatically captured and processed data is reported. All data is reported in micrometers. With measured porosity and grain Diameter, then applying modified Carmen & Kozeny formula to measure the abstract permeability (k_{abs})

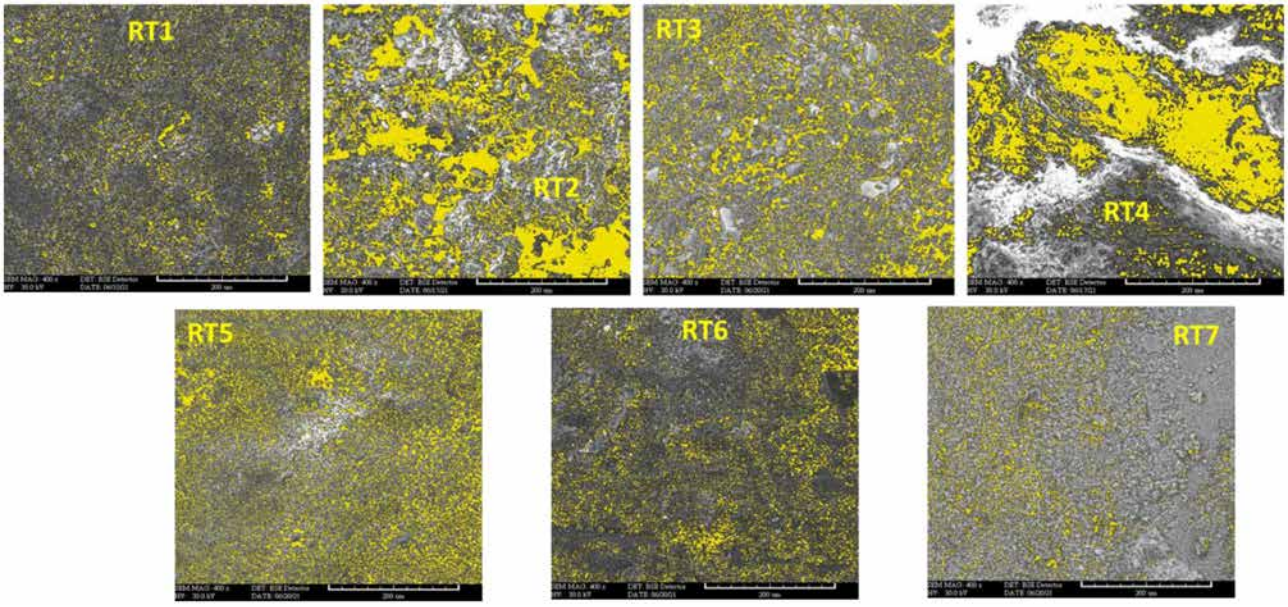

Figure 19—LIMESTONE selected 7 rock types porosity maps.

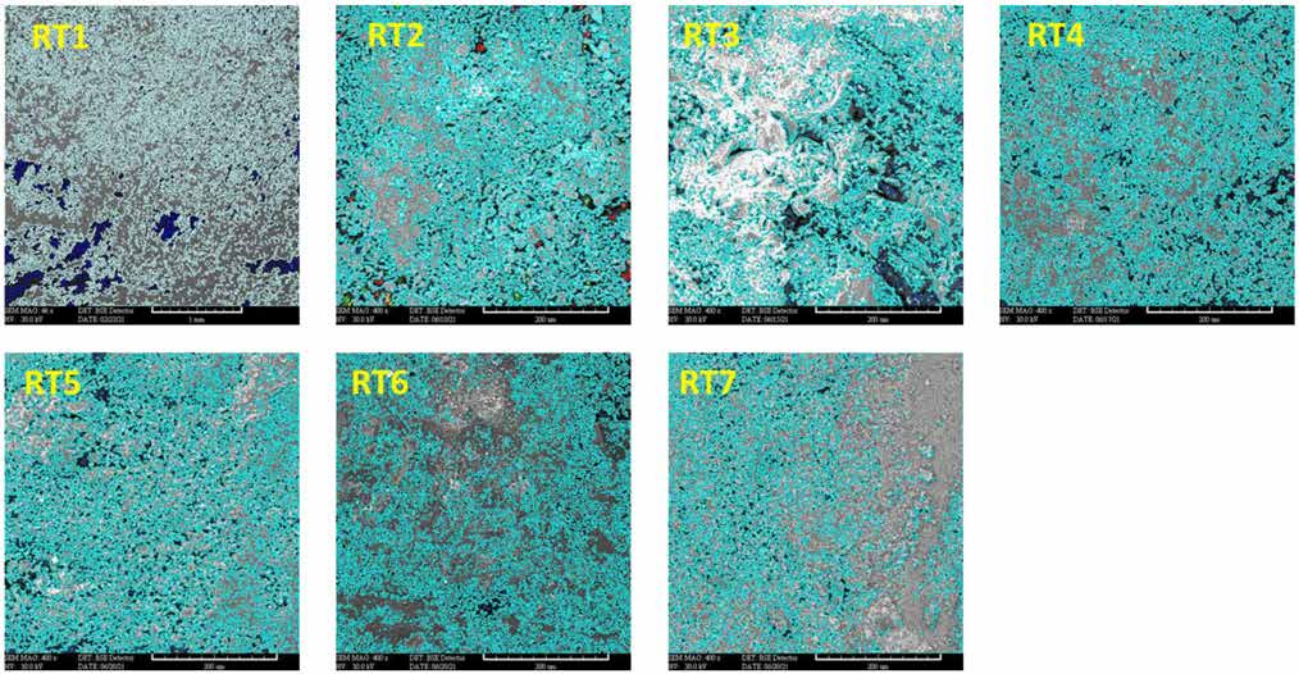

Figure 20—LIMESTONE selected 7 rock types grain diameter maps.

Table 5—Porosity calculations and absolute permeability calculations.

Rock Type RT Name	RT#	Reasons for Selection	Wettability Preference	Sample No.	Rock Type	Depth (ft)	Laboratory Routine Core Data				Scanned 2D Digital Image at 400X		
							GD	Kair (Amb)	K∞ (Amb)	Ø (Amb)	Ø (Matrix Only) Pore Area	All Grain Mean Equiv. diameter	Digital Absolute Permeability Carmen & Kozeny
							gm/cc	mD	mD	%	%	um	mD
A	1	Dolomite, tight matrix	MWW	1	RT1	7684.2	2.84	0.0001	0.0001	4.9	8.7	1.676	0.0125
A	1	maximum perm	SWW	2	RT1	7688.4	2.69	15.1	13.1	18.5	18.3	23.459	28.4374
A	1	minimum perm	SWW	3	RT1	7700.4	2.69	0.0001	0.0001	1.5	3.0	1.8	0.0005
A	1	maximum por	MWW	4	RT1	7708.6	2.69	11.1	8.73	23.1	10.2	2.558	0.0485
B	2	Tight Matrix	MWW	5	RT2	7713.25	2.7	0.0001	0.0001	5.2	15.9	2.158	0.1490
B	2	maximum perm	MWW	6	RT2	7718.45	2.67	23.6	20.5	26.1	16.4	2.631	0.2459
B	2	maximum por	WWW	7	RT2	7720.2	2.64	2.42	1.64	32.9	32.7	2.731	3.2405
B	2	KOC Selection	SWW	26**	RT2	7721.9	2.69	6.15	4.56	27.3	22.2	4.052	1.6703
B	2	minimum perm	MWW	8	RT2	7735.3	2.71	0.0001	0.0001	2.6	3.3	3.252	0.0023
C	3	minimum perm	MWW	9	RT3	7741.45	2.7	0.0001	0.0001	3.6	4.8	3.463	0.0082
C	3	maximum perm	MWW	10	RT3	7755.2	2.62	35	26.1	16.4	17.0	2.352	0.2220
C	3	maximum por	MWW	11	RT3	7759.85	2.71	5.85	3.83	25.1	22.0	12.203	0.0000
C	3	KOC Selection	MWW	27**	RT3	7767.1	2.69	5.16	4.37	20.9	21.1	2.507	0.5338
C	3	Dolomite	MWW	12	RT3	7773.8	2.72	4.51	4	14.1	17.4	2.5	0.2716
D	4	maximum GD	MWW	13	RT4	7777.7	2.74	7.82	6.03	20.2	21.4	2.65	0.6270
D	4	maximum por	MWW	14	RT4	7806	2.69	16	12.6	27.2	28.5	3.548	3.2081
D	4	maximum perm	MWW	15	RT4	7820.75	2.7	86	71	19.9	19.4	2.029	0.2604
D	4	minimum perm	MWW	16	RT4	7828.9	2.7	0.0001	0.0001	4.4	6.8	1.982	0.0080
E	5	maximum perm	MWW	17	RT5	7838.95	2.71	78.6	70.3	19.1	22.1	2.861	0.8194
E	5	Dolomite	MWW	18	RT5	7848	2.88	1.7	1.19	14.2	18.3	3.401	0.5977
E	5	maximum por	MWW	19	RT5	7854.4	2.7	5.46	3.9	25	24.7	4.884	3.5679
E	5	minimum perm	MWW	20	RT5	7878.2	2.71	0.0001	0.0001	6.2	10.7	1.864	0.0300
F	6	maximum por	MWW	21	RT6	7887.8	2.71	6.57	5.05	21.6	21.8	2.78	0.7369
F	6	maximum perm	MWW	22	RT6	7889.7	2.7	13.1	12.2	8.6	13.4	2.817	0.1433
F	6	minimum perm, Tight matrix	SWW	23	RT6	7918.3	2.67	0.0001	0.0001	1.8	5.7	4.136	0.0201
G	7	minimum perm, Tight matrix	MWW	24	RT7	7926.5	2.69	0.0001	0.0001	2.2	3.0	11.859	0.0227
G	7	maximum perm, maximum por	SWW	25	RT7	7933.8	2.71	0.481	0.366	8.9	8.5	3.541	0.0518

Table 6—Average wettability contact angles for the 7 rock types and the overall vertical average contact angle representation.

Rock Type	A	B	C	D	E	F	G	Overall LIMESTONE Average
Averaged θ° @400X magnification from table 4	33.3°	42.5°	40.2°	43.2°	37.6°	27.3°	29.3°	36.2°

Calculation of irreducible water saturation (S_{wirr}) and residual oil saturation (S_{or})

Big data for the scanned, captured and measured angles in all 7 rock types and in all 27 selected samples are portrayed for each measured average contact angle available inside the area captured showing number of angles counted for the designated area (Table 4 and 6). The 10 class areas have shown different wettability angles (Table 7). Class 1 pores show strong water wetness and angles are most likely the S_{wc}. Class 10 are pores that show oil wetness, therefore, S_{or}. These measured values are used in the relative permeability model.

Table 7—An example of rock sample #1 of rock type #1 with captured 10 classed contact angle distributions spanning from θ° (0° - 360°).

sample 1	Depth: 7684.2 ft		40X			400X			4000X		
		classes	Average Contact Angle	Angle Area	Number of Angles	Average Contact Angle	Angle Area	Number of Angles	Average Contact Angle	Angle Area	Number of Angles
		Sequence	θ°	µm^2	counts	θ°	µm^2	counts	θ°	µm^2	counts
		1	0.291	59.686	12868	0.729	1.162	3951	0.761	0.018	784
		2	48.477	157.052	266	51.935	7.505	207	50.177	0.38	25
		3	89.939	109.708	458	90.047	4.776	453	89.765	0.122	55
		4	131.665	176.765	291	127.387	13.768	286	129.426	0.514	32
		5	162.357	314.868	222	160.042	20.615	140	163.707	0.264	25
		6	198.576	308.897	201	199.574	15.944	145	201.375	0.896	12
		7	229.213	186.049	202	230.263	11.323	179	232.297	0.299	31
		8	269.864	118.686	229	268.487	4.822	290	269.324	0.399	54
		9	311.178	218.565	206	307.272	12.893	208	307.622	0.449	38
		10	342.611	336.24	248	340.644	16.952	144	341.71	0.441	17

Estimation of 2D digital Krw and Kro

Seven rock types and 27 samples are considered for this analysis. Three models were performed: Mohammed Ibrahim/ Koederitz, Honapour/Koederitz/Harvey, and Global Data which are shown in Figure 21 and Figures 29-30. The best model was Mohammed Ibrahim/Koederitz for low permeability rocks with small pore spaces that is believed to be controlled by pore geometry and water wet systems as in the case of LIMESTONE. The LIMESTONE shows strong to medium water wet system (Tables 6–10). Figure 28 shows a novel 2D digital imaging technology for estimating two-phase relative permeability in LIMESTONE. Also, Hearn PseudoRelative Permeability Empirical Equations Analysis (Honapour/ Koederitz/ Harvey) for estimating two-phase relative permeability in LIMESTONE is presented in figure 30.

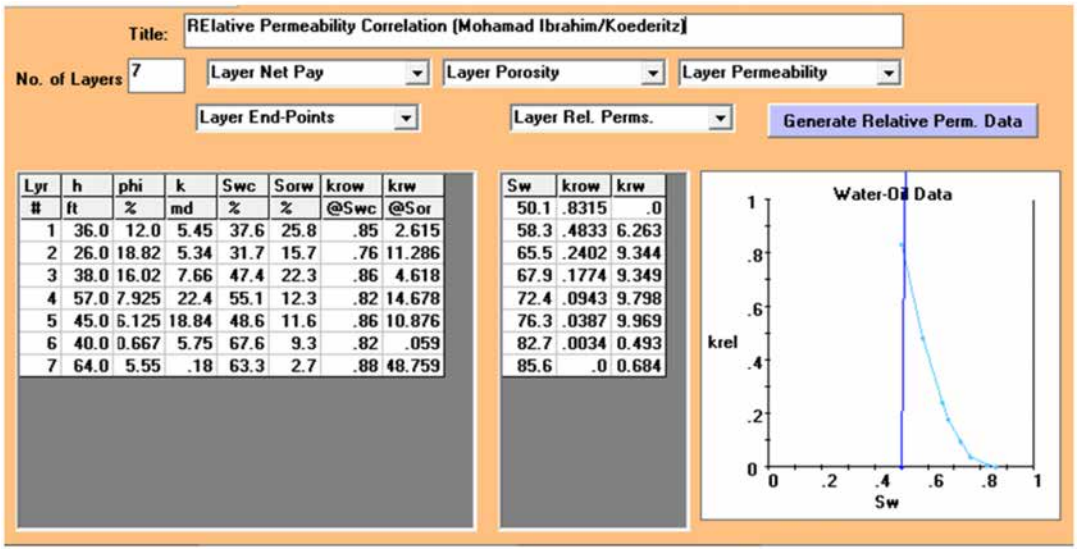

Lyr #	h ft	phi %	k md	Swc %	Sorw %	krow @Swc	krw @Sor
1	36.0	12.0	5.45	37.6	25.8	.85	2.615
2	26.0	18.82	5.34	31.7	15.7	.76	11.286
3	38.0	16.02	7.66	47.4	22.3	.86	4.618
4	57.0	7.925	22.4	55.1	12.3	.82	14.678
5	45.0	6.125	18.84	48.6	11.6	.86	10.876
6	40.0	0.667	5.75	67.6	9.3	.82	.059
7	64.0	5.55	.18	63.3	2.7	.88	48.759

Sw	krow	krw
50.1	.8315	.0
58.3	.4833	6.263
65.5	.2402	9.344
67.9	.1774	9.349
72.4	.0943	9.798
76.3	.0387	9.969
82.7	.0034	0.493
85.6	.0	0.684

Figure 21—Summary of index E: novel 2D digital imaging technology for estimating two-phase relative permeability in LIMESTONE for the 7 rock types.

Validation of relative permeability data from dynamic special core data

This data is supplied by Kuwait Oil Company (KOC) to act as a validation of our method. Samples 34-T, 65, and 94 were simulated for Brook's Corey relative permeability model, and the validation is satisfying with the 2D digital method technology.

Figure 22-23 shows the data provided by KOC for special core analysis (SCAL) on basic reservoir properties for laboratory relative oil and water end-point data. Figure 22 shows the Brooks-Corey relative oil and water curves as well as the fractional flow based on data in Figure 23. Figures 22-23 is the overlay of these relative curves and fractional flow (respectively) showing ideal conditions and a similar pattern for 3 different rock types. This observation suggests that all 3 rock types behave the same, which is highly unlikely knowing these rock types have different porosity, permeability, grain density, and lithology.

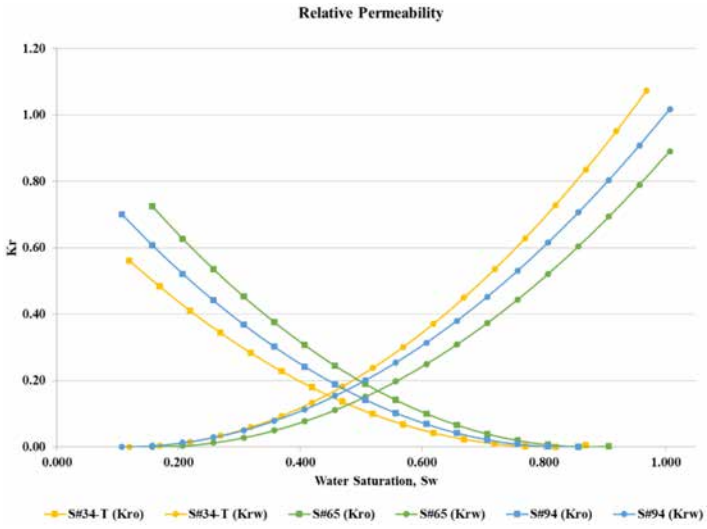

Figure 22—LIMESTONE dynamic SCAL relative permeability samples #34-T (RT #2), #65 (RT #3), and #94 (RT #4).

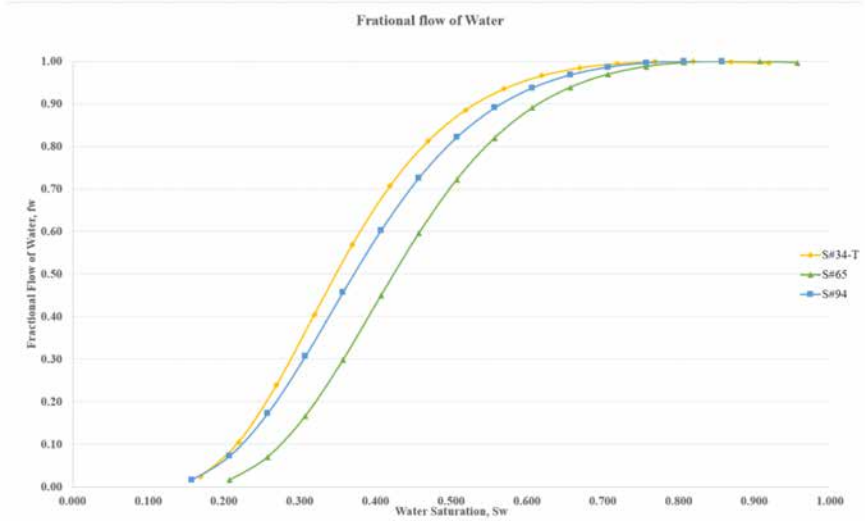

Figure 23—LIMESTONE dynamic SCAL fractional flow samples #34-T (RT #2), #65 (RT #3), and #94 (RT #4).

The novel method (pore imaging) had different results. Therefore, another overlay technique is carried out to compare differences and similarities between the two techniques for samples in RT #2, RT #3, and RT #4 as shown in Figures 24–26.

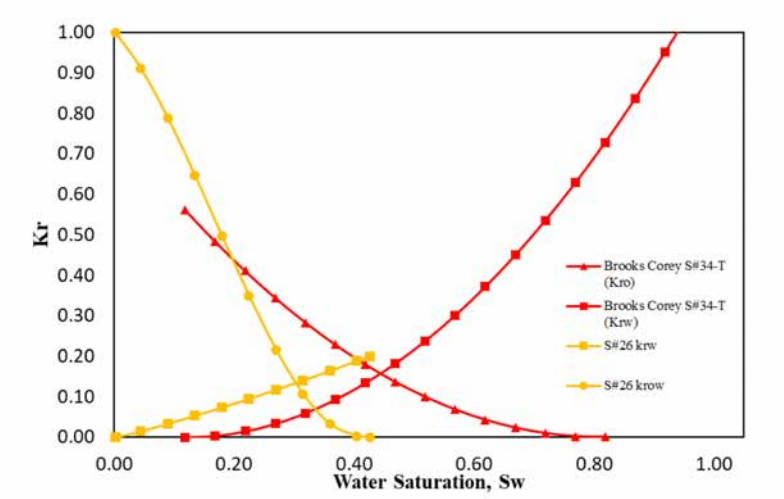

Figure 24—Overlay Corey model Vs digital relative permeability model for sample 7721.9 ft (RT #2).

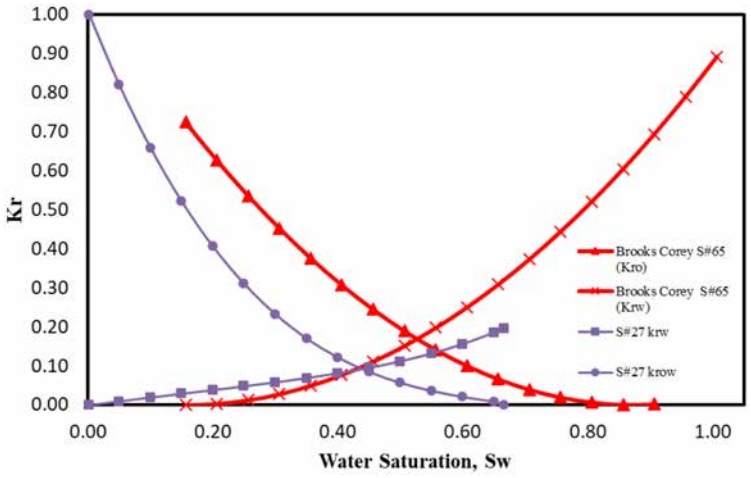

Figure 25—The overlay Corey model Vs digital relative permeability model for sample 7767.7 ft (RT #3).

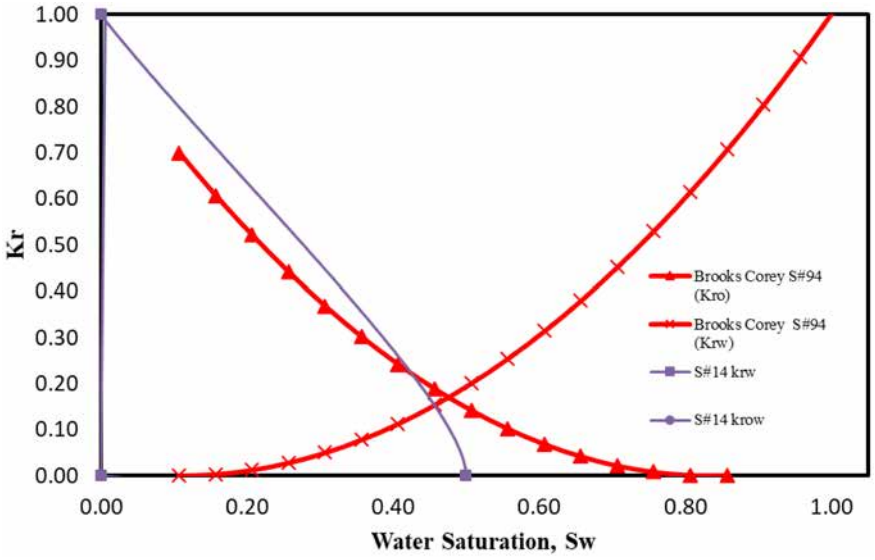

Figure 26—The overlay Corey model Vs digital relative permeability model for sample 7806 ft (RT #4).

The overlay model for sample #34T in Figure 24 shows that Brooks-Corey has a bigger scale (cm) with limited access to nanopores or isolated pores, so the recovery comes from only micrometer pores or higher. While the digital imaging models honor flow regimes in nanometer as well as the micrometer-scale pores. The endpoints are different because of scale issues, however, both approaches can complement each other. The researchers' opinion is that both graphs are important to understand the flow regime from pores of nanometer sizes to the centimeter scales. An integration of both methods can attempt to cover a wider size spectrum of pore shapes, and thus, more interesting fluid flow scenarios can be analyzed. The digital approach has the key advantage of explaining the unconventional tightness of carbonate reservoirs.

The overlay model for sample #65 in Figure 25 has total agreement relative permeability curve trends for both Brooks-Corey model as well as the digital model. The shift in the digital approach towards the left is because of nano-scale pores that Brooks-Corey cannot explain. The digital approach has the advantage of capturing the contact angle wettability; therefore, the digital approach has accuracy over the Brooks-Corey model where the wettability of the sample is completely ignored.

The overlay model for sample #94 in Figure 26 shows a discrepancy in the fracture of the rock sample between Brooks-Corey model and the digital novel. The selection of the sample that was in the conventional SCAL laboratory was based on a high permeability zone. This selection failed to explain that this optimistic streak of high permeability was due to a natural fracture, which was not detected at the time of sample selection. Now in this study the depth of 7806 shows that this zone has a noticeable natural fracture, and the novel digital approach has captured this fracture when the relative permeability curves are produced it shows the true shape of curves at the fracture zone. Usually, at conventional SCAL laboratories, the fractured zone is avoided. The advantage of this novel digital approach is the attempt of producing relative permeability curves for a fractured zone. This research study has yielded breakthrough new information about oil/water behavior in fractured zones.

Discussion and Recommendations

In North Kuwait LIMESTONE, table 8 shows the conventional pore system (40X) has an Average Contact Angle θ° of RT6 and RT7 scored less than 30°, which suggests a strong water-wet system. The RT1-RT2-RT3-RT4-and RT5 are all medium water wet (MWW).

Table 8—Conventional pore system.

40X							
	RT1	RT2	RT3	RT4	RT5	RT6	RT7
Average Contact angle θ°	33.3	42.5	40.2	43.2	37.6	27.3	29.3
Total Area Investigated µm^2	385.9	589.7	437.4	496.3	249.9	180.1	132.5
Total of Angles Measured	46,741	46,619	87,493	76,556	73,488	33,329	28,366

In North Kuwait LIMESTONE, table 9 shows the pore-throat system (400X) has an Average Contact Angle θ° of scores above 45° and less than 65°, which suggests MWW system. This observation is obtained in all rock types RT1-RT2-RT3-RT4-RT5-RT6 and RT7 are all MWW.

Table 9—Pore-throat pore system.

400X							
	RT1	RT2	RT3	RT4	RT5	RT6	RT7
Average Contact angle θ°	61.7	60.4	65.3	64.0	60.6	55.7	45.5
Total Area Investigated µm^2	33.8	119.1	36.3	149.3	16.8	10.0	4.9
Total of Angles Measured	33,262	30,790	22,418	37,528	34,322	24,725	11,120

In North Kuwait LIMESTONE, table 10 shows the unconventional nano pore system (4000X) has an Average Contact Angle θ° scores above than 32° and less than 50°, which suggests MWW. This observation is obtained in all rock types RT1-RT2-RT3-RT4-RT5-RT6 and RT7 are all MWW.

Table 10—Unconventional tight nano pore system.

4000X							
	RT1	RT2	RT3	RT4	RT5	RT6	RT7
Average Contact angle θ°	49.0	36.0	46.6	47.0	40.2	32.7	32.9
Total Area Investigated µm^2	2.0	3.4	2.9	3.4	1.0	0.4	0.2
Total of Angles Measured	10,008	10,725	5,617	18,265	8,250	8,557	4,616

The contact angles from different resolution images lead to different answers as presented in Figure 27, and they do not agree with each other. This disagreement is because of the scale and size-area of pores investigated, pore/wall boundary contact angle wettability distribution, and morphology issues such as pore, length, width, roundness and elongation, area, perimeter, and equivalent diameter. If the study addresses reservoir matrix tightness as well as isolated pores, then 4000X is accepted for wettability contact angle representation (Table 10) because of capturing nano-pores. When connectivity and pore throat representation are considered, then 400X might be the right model to represent the wettability inside the pore throat corridors, which is usually in micrometer scale (Table 9). However, the largest scale 40X scale includes all rock pore systems available in the captured image, so it includes the conventional pore system, pore throats, and unconventional tight nano pores therefore, Table 8 is the representation of contact angle wettability of pore body captured in millimeter scale for the rock types samples.

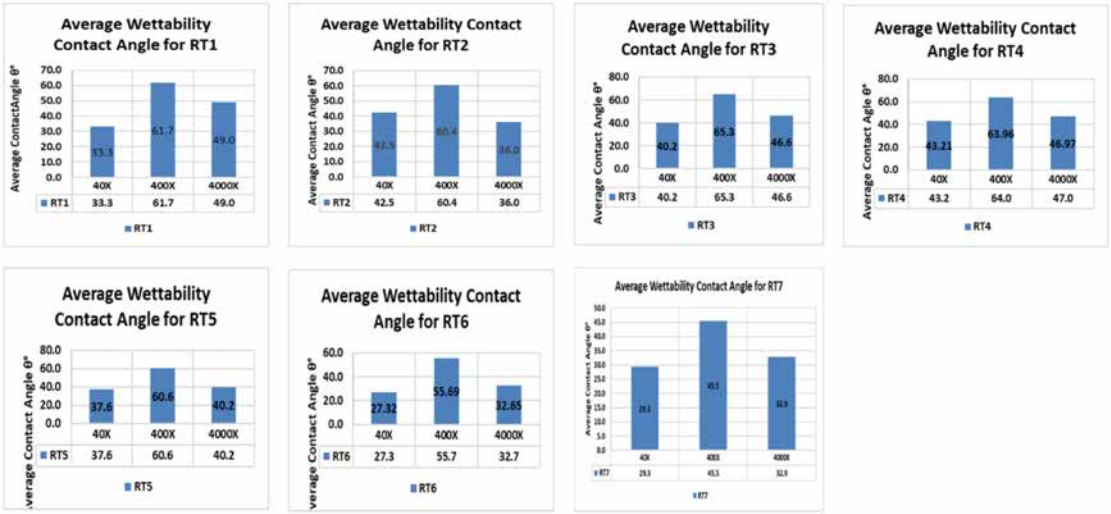

Figure 27—Wettability contact angle distributions for the 7 rock types.

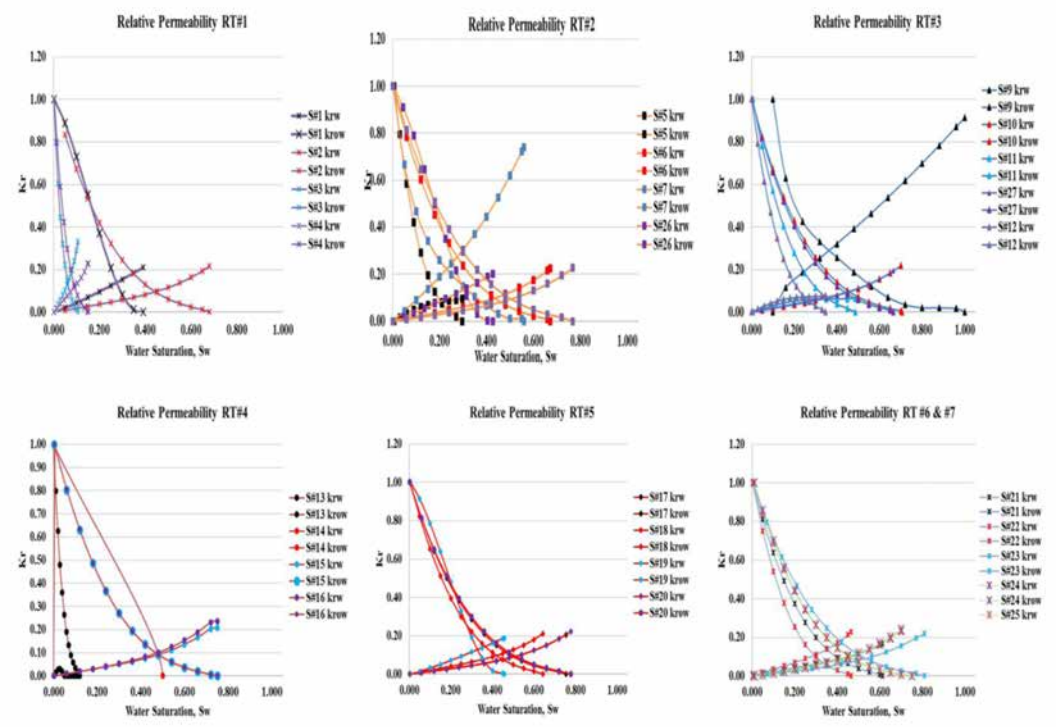

Figure 28—The practical 2D digital imaging of the LIMESTONE 7 rock types.

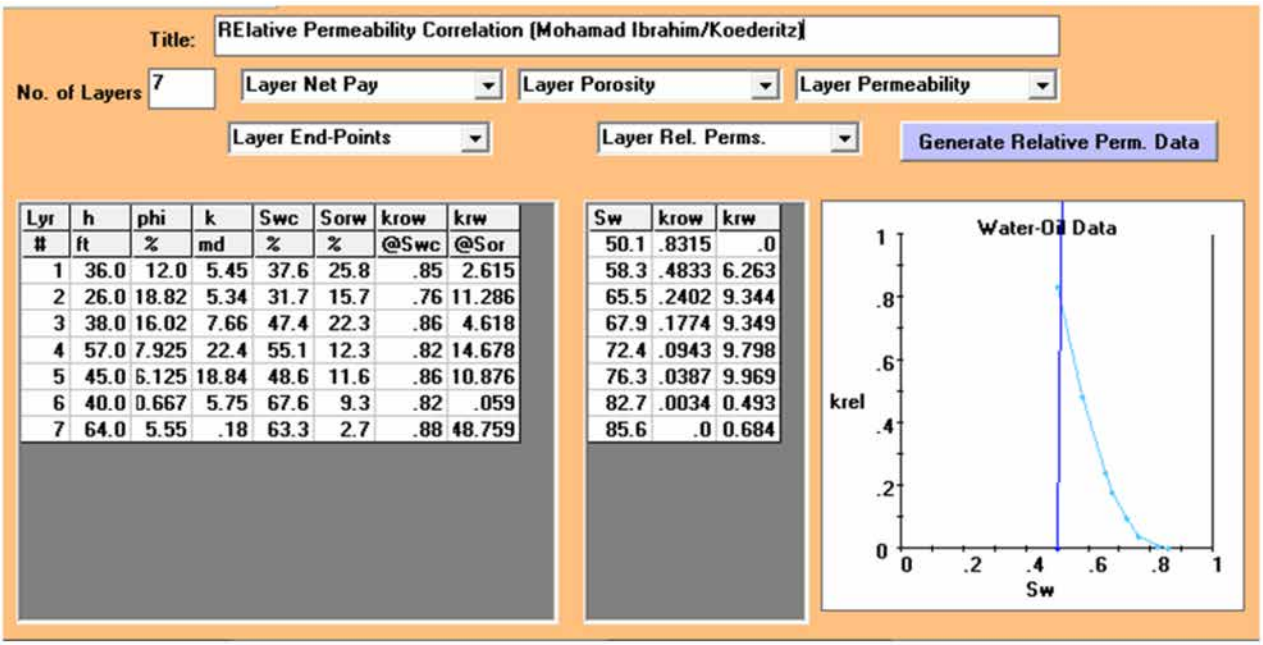

Lyr #	h ft	phi %	k md	Swc %	Sorw %	krow @Swc	krw @Sor
1	36.0	12.0	5.45	37.6	25.8	.85	2.615
2	26.0	18.82	5.34	31.7	15.7	.76	11.286
3	38.0	16.02	7.66	47.4	22.3	.86	4.618
4	57.0	7.925	22.4	55.1	12.3	.82	14.678
5	45.0	6.125	18.84	48.6	11.6	.86	10.876
6	40.0	0.667	5.75	67.6	9.3	.82	.059
7	64.0	5.55	.18	63.3	2.7	.88	48.759

Sw	krow	krw
50.1	.8315	.0
58.3	.4833	6.263
65.5	.2402	9.344
67.9	.1774	9.349
72.4	.0943	9.798
76.3	.0387	9.969
82.7	.0034	0.493
85.6	.0	0.684

Figure 29—Hearn pseudorelative permeability analysis (Mohamad Ibrahim/Koederitz) for the entire thickness and entire 7 rock types.

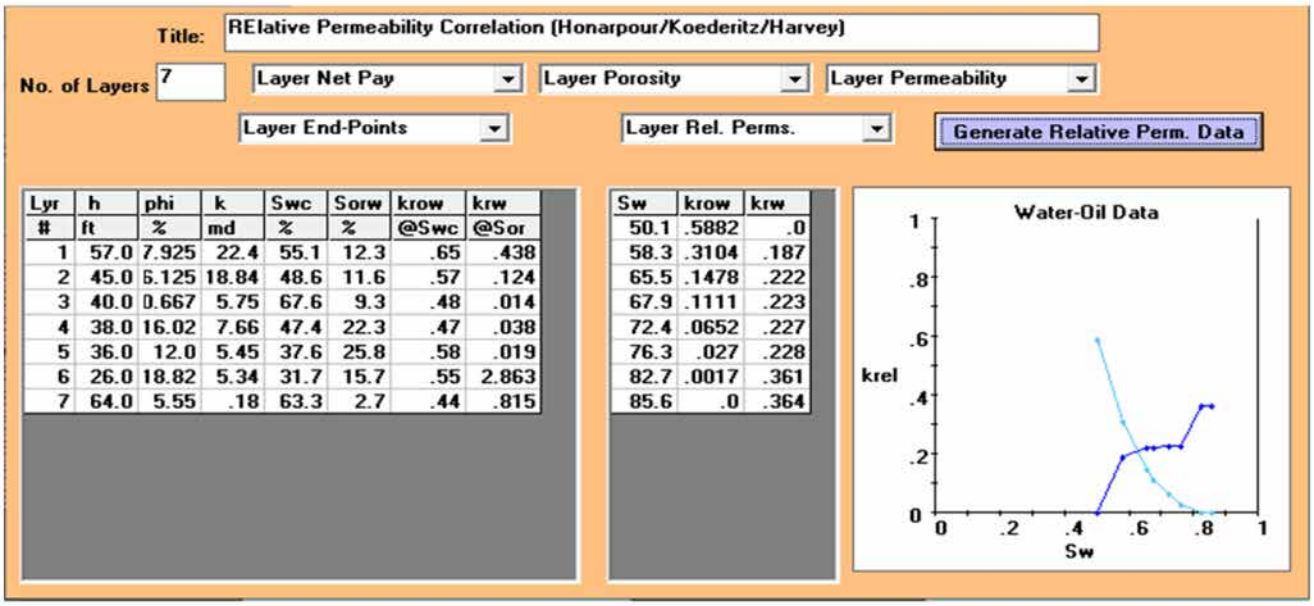

Lyr #	h ft	phi %	k md	Swc %	Sorw %	krow @Swc	krw @Sor
1	57.0	7.925	22.4	55.1	12.3	.65	.438
2	45.0	6.125	18.84	48.6	11.6	.57	.124
3	40.0	0.667	5.75	67.6	9.3	.48	.014
4	38.0	16.02	7.66	47.4	22.3	.47	.038
5	36.0	12.0	5.45	37.6	25.8	.58	.019
6	26.0	18.82	5.34	31.7	15.7	.55	2.863
7	64.0	5.55	.18	63.3	2.7	.44	.815

Sw	krow	krw
50.1	.5882	.0
58.3	.3104	.187
65.5	.1478	.222
67.9	.1111	.223
72.4	.0652	.227
76.3	.027	.228
82.7	.0017	.361
85.6	.0	.364

Figure 30—Digital pseudorelative permeability analysis (Honapour/ Koederitz/Harvey) for the entire thickness and entire 7 rock types.

Conclusions

North Kuwait LIMESTONE is a tight carbonate (fair matrix porosity of about 9.7% and low matrix horizontal permeability of about 0.36 mD), which has 7 rock type zones (A, B, C, D, E, F, and G) where F and G at bottom of hydrocarbon zones have the lowest porosity and permeability. LIMESTONE also has thief zones (Fractures), which are responsible for water production and strong oil wettability. There are 3 main grain minerals in LIMESTONE to make the heterogeneities more complex: Limestone, Dolomite, and Sandstone, which all were confirmed in the permeability architectures of this LIMESTONE.

A, B, C, D, and E zones are 5 broader rock types with different porosity and permeability henceforth better oil recoveries than F and G zones. Many digital relative permeability based on digital wettability models are developed. Global relative permeability data from many reservoirs around the world are surveyed and show that there are several scenarios for this LIMESTONE relative permeability curve developments, and they often yield useful responses for primary as well as secondary recovery.

Another method of determining relative permeability is reservoir rock imaging analysis. This method is commonly known as the wettability morphology model. This study utilizes the morphology of pore types by counting 2D scale big measured data contact angle Method. 27 samples have been selected for this study to represent the entire thickness and the entire 7 rock types spanned over 306 feet of vertical depth.

The BSE-SEM instrument has successfully developed 162 images, which all are successfully processed for porosity, grain diameter, absolute permeability, wettability contact angle, and initial water saturation S_{wc}, residual oil saturation S_{or}, and water and oil relative permeabilities K_{rw} and K_{ro}.

Big Data was yielded and a 2D digital artificial intelligence model is developed. The total average of the contact angle wettability yielded at $\theta = 36.2°$, which according to the Al-Bazzaz wettability classification is considered as a medium water wet spanning over 7 layers A to G for 306 feet. The relative permeability curves of rock type 4 (RT4) and specifically in rock samples 13 and 14 have not yielded accurate estimates, and that is because of fractures in the samples. Also, it is known from routine and special core analyses that RT4 has the highest porosity and permeability due to fractures. However, the small scale of imagining methods has successfully capture the matrix relative permeability curves for these RT4 samples #13 and #14 without crossing any existing fractures. This method indicates that imaging techniques are not only low cost and fast data retrieval but also accurate in capturing the physics at finite levels.

Acknowledgments

This research has been totally financed by the Innovation and Technology (INT) team at Kuwait Oil Company Contract: PP00S168S. The study team would like to thank Kuwait Oil Company (KOC) for providing us with necessary information as well as reservoir rock samples. The KOC team is divided into three teams: team KOC-North Kuwait (The end-user) lead by Dr. Chao Chen, Team-A KOC-R&T (The technical) lead by Dr. Ali Qubian and Mr. Abdulaziz Safar, and Ms. Nora Al-Kudhair. Also, Team-B KOC-INT (The management) lead by Mr. Hamad Al-Rashedi and Mr. Mohammed Al-Senafy. Also, the study team would like to extend thanks to KISR management and support, Dr. Dawood Bahzad and Dr. Abdulhameed Al-Hashem for management, support and patience. The team also would like to thank Ms. Suraiya Bandarkar for her cooperation and coordination.

References

1. M. B. Alotaibi, R. Azmy, H. A. Nasr-El-Din, Texas A&M U., Wettability Challenges in Carbonate Reservoirs, SPE Improved Oil Recovery Symposium, 24-28 April, 2010, Tulsa, Oklahoma, USA. DOI: https://doi.org/10.2118/129972-MS.
2. A.G. Mitchell, L.B. Hazell, and K.J. Webb, British Petroleum, Wettability Determination: Pore Surface Analysis, SPE Annual Technical Conference and Exhibition, 23-26 September, New Orleans, Louisiana, USA. DOI: https://doi.org/10.2118/20505-MS.
3. N. R. Morrow, New Mexico Petroleum Recovery Research Center, New Mexico Inst. of Mining & Technology, Wettability and Its Effect on Oil Recovery, SPE-21621-PA, Society of Petroleum Engineers, *Journal of Petroleum Technology*, 1 December, 1990. DOI: https://doi.org/10.2118/21621-PA.
4. K.J. Webb, C.J.J. Black, BP Exploration, UK, T. Namba, ZADCO, Abu Dhabi, UAE, Resolving Wettability in a Giant Carbonate Reservoir, SPE-36257-MS, Society of Petroleum Engineers, Abu Dhabi International Petroleum Exhibition and Conference, 13-16 October, 1996, Abu Dhabi, United Arab Emirates. DOI: https://doi.org/10.2118/36257-MS.
5. Rao, Dandina N., Petroleum Recovery Institute, Wettability Effects in Thermal Recovery Operations, SPE-35462-MS, Society of Petroleum Engineers, SPE/DOE Improved Oil Recovery Symposium, 21-24 April, 1996, Tulsa, Oklahoma, USA. DOI: https://doi.org/10.2118/35462-MS.
6. R. Gupta, and K. K.Mohanty, U. of Houston, Wettability Alteration of Fractured Carbonate Reservoirs, SPE-113407-MS, SPE Conference Paper, SPE Symposium on Improved Oil Recovery, 20-23 April, 2008, Tulsa, Oklahoma, USA. DOI: https://doi.org/10.2118/113407-MS.
7. G. Hamon, ELF Exploration Production, Field-Wide Variations of Wettability, SPE-63144-MS, SPE Conference Paper, SPE Annual Technical Conference and Exhibition, 1-4 October, 2000, Dallas, Texas, USA. DOI: https://doi.org/10.2118/63144-MS.
8. AlHakeem, K. Liu, University of Missouri Science & Technology, W. H. Al-Bazzaz, Kuwait Institute for Scientific Research, Up-Scaled Petrophysical Analyses Using Micro-Level Field-Of-View Petrographic Images for the Kapuni Group, Taranaki Basin, New Zealand, Search and Discovery Article #10953 (2017), Adapted from extended abstract based on poster presentation given at AAPG June 19, 2017, Annual Convention and Exhibition, Houston, Texas, United States, April 2-5, 2017.
9. Up-Scaled Petrophysical Analyses Using Micro-Level Field-Of-View Petrographic Images for the Kapuni Group, Taranaki Basin, New Zealand | Request PDF. Available from DOI: https://www.researchgate.net/publication/321746768_Up-scaled_Petrophysical_Analyses_Using_Micro-Level_Field-Of-View_Petrographic_Images_for_the_Kapuni_Group_Taranaki_Basin_New_Zealand [accessed Oct 14 2018].

10. W. G. Anderson, Conoco Inc., Wettability Literature SurveyPart2: Wettability Measurement, Original manuscript received in the Society of Petroleum Engineers office Dec, 28, 1984, Paper (SPE 13933 PA) accepted for publication July 23, 1985, Revised manuscript received March 3, 1986, *JPT*.
11. J. S. Buckly, Petroleum Recovery Research Center, New Mexico Institute of Mining and Technology, EVALUATION OF RESERVOIR WETTABILITY AND ITS EFFECT ON OIL RECOVERY, *First Annual Report, U.S. Department of Energy*, July 1, 1996 - June 30, 1997.
12. E. C. Donaldson and W. Alam, Wettability, Copyright © 2008 Gulf Publishing Company, Houston, Texas, USA, 2008. ISBN- 10: 1-933762-29-2, ISBN- 13: 978-1-933762-29-6.
13. Atlas TM Software, TESCAN Digital Microscopy Imaging, Atlas Main Executable, Version 2.9.1.0, Libu ina t.21, 62300 Brno, *Czech Republic*, May 2000.
14. W. H. Al-Bazzaz and Y. W. Al-Mehanna, Porosity, Permeability, and MHR Calculator Using SEM & Thin Section for Characterizing Complex Limestone-Burgan Carbonate Reservoir. Presented at Society of Petroleum Engineers Conference, SPE 110730, held at Asia Pacific Oil and Gas Conference and Exhibition, 30 October-1 November, 2007, Jakarta, Indonesia 2007. DOI: https://doi.org/10.2118/110730-MS.
15. Honapour, M., Koederitz, L.F., and Harvey, A.H.: "Empirical Equations for Estimating Two-Phase Relative Permeability in Consolidated Rock," *JPT* (December 1982) **34**, 2905–2908.
16. Honapour, M., Koederitz, L.F., and Harvey, A.H.: *Relative Permeability of Petroleum Reservoirs*, CRC Press, Inc., Boca Raton (1986).
17. Honapour, M., & Mahmood, S. M. (1988). Relative-Permeability Measurements: An Overview. *Journal of Petroleum Technology*, **40**(08), 963–966. doi:10.2118/18565-pa.
18. Zhao, B., Ratnakar, R., Dindoruk, B., & Mohanty, K. (2020). A Hybrid Approach for the Prediction of Relative Permeability Using Machine Learning of Experimental and Numerical Proxy SCAL Data. *SPE Journal*. doi:10.2118/196022-pa.
19. Alpak, F. O., Lake, L. W., & Embid, S. M. (1999). Validation of a Modified Carman-Kozeny Equation to Model Two-Phase Relative Permeabilities. SPE Annual Technical Conference and Exhibition. doi:10.2118/56479-ms.
20. Al Ibrahim, Mustafa A., Kerimov, Abdulla, Mukerji, Tapan, and Gary Mavko. "Digital rocks with irregularly shaped grains: A simulator tool for computational rock physics." Paper presented at the 2018 SEG International Exposition and Annual Meeting, Anaheim, California, USA, October 2018. doi: https://doi.org/10.1190/segam2018-2993373.1.
21. Pandey, V. J., Itibrout, T., Adams, L. S., Cowan, T. L., & Bustos, O. A. (2007). Fracture Stimulation Utilizing a Viscoelastic Surfactant Based System in the Morrow Sands in Southeast New Mexico. International Symposium on Oilfield Chemistry. doi:10.2118/102677-ms.
22. Gao, Y., Raeini, A. Q., Blunt, M. J., & Bijeljic, B. (2019). Pore Occupancy, Relative Permeability and Flow Intermittency Measurements Using X-Ray Micro-tomography in a Complex Carbonate. *Advances in Water Resources*. doi:10.1016/j.advwatres.2019.04.0.
23. Qingyang Lin, Takashi Akaia, Martin J. Blunt, Branko Bijeljic, Hiroki Iwama, Katsumo Takabayashi, Yutaka Onaka, Hideharu Yonebayashi. Pore-scale imaging of asphaltene-induced pore clogging in carbonate rocks. Published by Elsevier Ltd. *This is an open access article under the CC BY-NC-ND license*. https://doi.org/10.1016/j.fuel.2020.118871.
24. Ahmed M. Selem, Nicolas Agenet, Ying Gao, Ali Q. Raeini, Martin J. Blunt & Branko Bijeljic. Pore-scale imaging and analysis of low salinity waterflooding in a heterogeneous carbonate rock at reservoir conditions. *Scientific Reports* | (2021) **11**:15063 Nature Portfolio. https://doi.org/10.1038/s41598-021-94103-w.

25. Schneider, F. N., & Owens, W. W. (1970). Sandstone and Carbonate Two- and Three-Phase Relative Permeability Characteristics. *Society of Petroleum Engineers Journal*, **10**(01), 75–84. doi:10.2118/2445-pa.
26. Eleri, O. O., Graue, A., & Skauge, A. (1995). Steady-State and Unsteady-State Two-Phase Relative Permeability Hysteresis and Measurements of Three-Phase Relative Permeabilities Using Imaging Techniques. SPE Annual Technical Conference and Exhibition. doi:10.2118/30764-ms.
27. Byrnes, A. P., Zhang, S., Canter, L., & Sonnenfeld, M. D. (2018). Application of Integrated Core and Multiscale 3-D Image Rock Physics to Characterize Porosity, Permeability, Capillary Pressure, and Two- and Three-Phase Relative Permeability in the Codell Sandstone, Denver Basin, Colorado. Proceedings of the 6th Unconventional Resources Technology Conference. doi:10.15530/urtec-2018-2901840.
28. McCaffery, F. G., & Bennion, D. W. (1974). The Effect OfWettability On Two-Phase Relative Penneabilities. *Journal of Canadian Petroleum Technology*, **13**(04). doi:10.2118/74-04-04.
29. Qingyang Lin, Branko Bijeljic, Sajjad Foroughi, Steffen Berg, Martin J. Blunt. Pore-scale imaging of displacement patterns in an altered-wettability carbonate. https://doi.org/10.1016/j.ces.2021.116464.
30. Waleed Al-Bazzaz, Salah AlMuddhhi, & Mohammed AlOstath. Investigation Wettability Contact Angle Measurement in Kuwaiti Heavy Oil Reservoir and Modeling Using 2D Imaging Technologies. SPE International Heavy Oil Conference and Exhibition. (2018). doi:10.2118/193706-ms.
31. Waleed Albazzaz, Salah Almudhhi, & Mohammed Alostath. Investigating wettability contact angle measurement in Kuwaiti heavy oil reservoir and modeling using 2D imaging technologies. *PETROL SCI TECHNOL*.
32. Salah Almudhhi, Mohammed Alostath, Waleed Al-Bazzaz, Hamied. Sharifigaliuk, & Ali Qubian. "An unconventional approach in investigating wettability contact angle measurement in shale resources." *PETROL SCI TECHNOL*, Vol. **40**, Issue 8, Pages 893–936. (2021). https://doi.org/10.1080/10916466.2021.2008969.
33. Waleed H. Al-Bazzaz, Yousef Al-Mehanna, & Anuj Gupta. Permeability Modeling Using Neural Network Approach for Complex Mauddud-Burgan Carbonate Reservoir. SPE Middle East Oil and Gas Show and Conference. (2007). doi:10.2118/105337-ms.
34. Hussain Alajaj, Ralph Flori, Saleh Alsayegh, Haidar Almubarak, Waleed Al-Bazzaz. Investigation of Pore Geometry Wettability Preference in an Oolitic Oil Reservoir: Pore Scale Imaging and Modelling Study. Society of Core Analysts, September, 2022, Austin, Texas, USA, DOI: 10.5281/zenodo.7087702.
35. Hamid Sharifigaliuk, Syed Mohammad Mahmood, Waleed Al-Bazzaz, Vahid Khosravi. Complexities Driving Wettability Evaluation of Shales toward Unconventional Approaches: A Comprehensive Review. January 2021, *Energy & Fuels* **35**(2), DOI: 10.1021/acs.energyfuels.0c03661.